Dual-Phase Lithium Metal Anode Containing a Polysulfide-Induced Solid Electrolyte Interphase and Nanostructured Graphene Framework for Lithium–Sulfur Batteries

Xin-Bing Cheng, Hong-Jie Peng, Jia-Qi Huang, Rui Zhang, Chen-Zi Zhao, and Qiang Zhang*

Beijing Key Laboratory of Green Chemical Reaction Engineering and Technology, Department of Chemical Engineering, Tsinghua University, Beijing 100084, China

ABSTRACT Lithium–sulfur (Li–S) batteries, with a theoretical energy density of 2600 Wh kg^{-1}, are a promising platform for high-energy and cost-effective electrochemical energy storage. However, great challenges such as fast capacity degradation and safety concerns prevent it from widespread application. With the adoption of Li metal as the anode, dendritic and mossy metal depositing on the negative electrode during repeated cycles leads to serious safety concerns and low Coulombic efficiency. Herein, we report a distinctive graphene framework structure coated by an *in situ* formed solid electrolyte interphase (SEI) with Li depositing in the pores as the anode of Li–S batteries. The graphene-based metal anode demonstated a superior dendrite-inhibition behavior in 70 h of lithiation, while the cell with a Cu foil based metal anode was short-circuited after only 4 h of lithiation at 0.5 mA cm^{-2}. The graphene-modified Li anode with SEI induced by the polysulfide-containing electrolyte improved the Coulombic efficiency to ~97% for more than 100 cycles, while the control sample with Cu foil as the current collector exhibited huge fluctuations in Coulombic efficiency. The unblocked ion pathways and high electron conductivities of frameworks in the modified metal anode led to the rapid transfer of Li ions through the SEI and endowed the anode framework with an ion conductivity of 7.81×10^{-2} mS cm^{-1}, nearly quintuple that of the Cu foil based Li metal anode. Besides, the polarization in the charge–discharge process was halved to 30 mV. The stable and efficient Li deposition was maintained after 2000 cycles. Our results indicated that nanoscale interfacial electrode engineering could be a promising strategy to tackle the intrinsic problems of lithium metal anodes, thus improving the safety of Li–S cells.

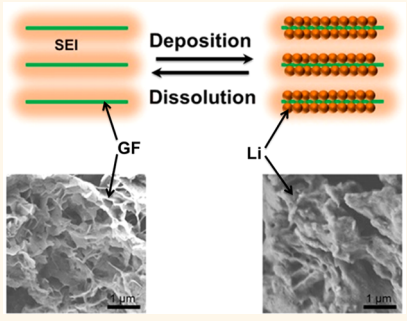

KEYWORDS: Li–S battery · anode · dendrite · graphene

Fossil fuels, one of the most convenient energy resources of chemical energy, are consumed in an extreme quantity and at a rapidly increasing rate.[1] Except for the significant contribution to the world economy, the combustion of fossil fuels is majorly responsible for air pollution and global warming. This "energy anxiety" raises an urgent need for environmentally friendly and sustainable energy sources. Many of the alternative energy sources (solar, wind, waves, geothermal sources, *etc.*) require advanced energy storage technology, such as batteries, to replace conventional fossil fuels. Among various promising battery candidates with high energy densities, lithium–sulfur (Li–S) batteries, with a high theoretical capacity of 1675 mAh g^{-1} (based on sulfur) and an energy density of 2600 Wh kg^{-1} (based on the lithium–sulfur redox couple), are highly considered.[2–4] Despite these advantages, many obstacles still need to be overcome for practical applications of Li–S batteries, such as the low conductivity of sulfur and the shuttle of long-chain polysulfide intermediates during discharge/charge cycling. During the past 10 years, various strategies have been proposed to address these issues in Li–S cells, such as nanostructured hosts,[5–14] conductive polymers,[15–17] and a bifunctional separator,[18–22] which improved the cycling performance to more than 1000 cycles with a Coulombic efficiency of 90–99% and discharge capacity of 500–800 mAh g^{-1}.[23–30] However, the superior cycling performance

* Address correspondence to zhang-qiang@mails.tsinghua.edu.cn.

Received for review April 2, 2015 and accepted June 4, 2015.

Published online June 04, 2015
10.1021/acsnano.5b01990

was mostly achieved by a 2000% lithium excess,[31] which hindered the problem of the Li metal anode. Generally, the formation of Li dendrites is a primary issue for Li metal batteries (LMBs) including Li−S batteries, which always leads to serious safety concerns and low Coulombic efficiency.

Dendrite formation on a metal lithium anode in a Li−S cell is an even more severe problem than it is for routine lithium ion cells. Unlike lithium ion cells, intermediate products (lithium polysulfides) are formed in the cathode and are soluble in the electrolyte, which is in direct contact with the metallic anode and therefore leads to a much more complicated system with the coexistence of Li dendrites and polysulfide intermediates. Recently, the anode issue of the effect of polysulfides[32,33] has attracted great attention, and some creative ideas to handle the dendrite problems in Li−S batteries, such as a $LiNO_3$ electrolyte additive,[34] a high-concentration Li salt,[35] solid-state electrolytes,[25] an all-carbon anode,[31] a hybrid anode structure,[36] a 3D Li_7B_6 nanofiber framework,[37,38] and a protected lithium anode,[39] have been proposed. These strategies provide bright prospects to improve the cycling and safety performance of Li−S batteries in view of the anode. However, the electrochemical behavior of the anode in a Li−S cell has rarely been involved. In fact, the electrochemistry of the anode is of vital importance to enhance the understanding of nucleation and growth of Li dendrites and their contribution to the whole cell device.

Generally, dendrite formation is mainly induced by inhomogeneous distribution of (1) the current density on the electrode surface and (2) the concentration gradient of Li ions at the electrolyte/electrode interface. The academic research on metallic Li anodes has never lagged in the past 40 years.[6,36,40−45] Several methods have been proposed to solve the dendrite problem including (1) the formation of Li−Al or Li−Mg alloys;[46,47] (2) the employment of a solid-state electrolyte;[48−52] (3) the introduction of a stable and protective solid electrolyte interphase (SEI);[18,39,53−57] (4) the incorporation of some electrolyte additive to manipulate the deposited Li,[25,58,59] and the application of a nanostructured anode through mechanical surface modification or fibrous scaffolds.[37,60,61] All these methods afford a mechanistic understanding into dendrite inhibition. However, Li metal based batteries are still stalled in proof-of-concept with few commercial attempts yet.

According to a recent interesting study on Li metal symmetric cells with a polymer electrolyte, most of the Li dendritic structures resided underneath the Li surface instead of growing out of the surface and piercing into the polymer electrolyte in the early stage of dendrite development.[62] This study revealed an "inward and recessive" structural evolution of the Li anode with potential significance for designing an advanced metallic anode, which was normally concealed by visible hazards carried out by "outward and dominant" Li dendrites. Similarly, Xiao *et al.* discovered a novel failure mechanism of Li metal anodes, that the porous interphase of the anode grew inward toward the bulk (fresh) Li metal, which evolved into a messy and highly resistive layer and, thus, resulted in huge transfer resistance and a great amount of Li metal losing contact with electrons (dead Li) in the inert layer. Before the dendrite-induced short circuit, the impedance of the battery escalated sharply and the service life was terminated early.[63] In a Li−S cell, this phenomenon is more frequent and serious, because sulfur and lithium sulfide products are both ion- and electron-insulating and the cross-coupling effect will lead to a sharp decrease in the voltage and energy density. Consequently, it is critically important to design an anode structure with desirable electron and ion channels to improve transfer properties and recycle dead Li in a Li−S cell.

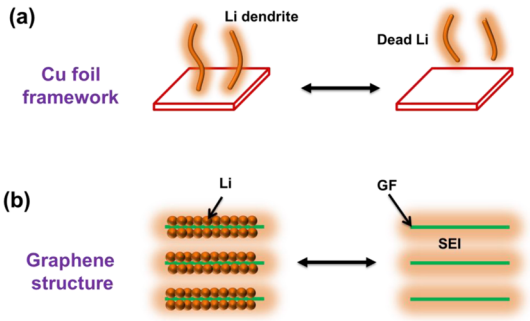

Figure 1. Schematic diagrams of a Li metal anode with different structures during Li deposition and dissolution. (a) Without a graphene framework, Li dendrites appear during Li deposition, thus leading to a large amount of dead Li during Li dissolution. (b) The SCG-structured anode depicts a stable and uniform Li deposition and dissolution with high efficiency and low resistance.

In this contribution, we propose a nanostructured graphene framework with Li deposition to be a high-efficiency and high-stability Li metal anode for Li−S batteries. In a routine configuration of a Li metal anode without a graphene framework, Li dendrites easily grew on routine two-dimensional (2D) substrates (such as Cu foil). As the root of dendrites can easily receive electrons and then dissolve early, Li dendrites easily fracture and detach from the substrate to form dead Li (Figure 1a). If there is a pre-existing conductive framework such as self-supported graphene foam, the deposited Li will be well accommodated (Figure 1b). Free-standing graphene foam provides several promising features as an underneath layer for a Li anode, including (1) relative larger surface area than 2D substrates to lower the real specific surface current density and the possibility of dendrite growth, (2) an interconnected framework to support and recycle dead Li, and (3) good flexibility to sustain the volume fluctuations during repeated incorporation/extraction of Li.

To build the working environment of Li−S cells, 0.1 M Li_2S_8 is added into the presented electrolyte. Several demonstrations on the Li anode reinforced by Li_2S_x ($x = 1-8$) enlightened a new prototype of a robust and stable SEI.[32,54,64] Consequently, polysulfides can be presented as the SEI stabilizer of the anode. The smooth layer covering the surface of the graphene nanosheets was presumably assigned to *in situ* formed SEI and was identified in a subsequent demonstration by X-ray photoelectron microscopy (XPS). The dual-phase layered structure composed of an *in situ* formed SEI and a nanostructured graphene framework and denoted as SEI-coated graphene (SCG) ensures the requirements on the Li metal from the two sides of the electrode/electrolyte interface and, thereby, enables highly efficient and stable utilization of Li−S batteries.

RESULTS AND DISCUSSION

SEM Characterization of Li Deposition and Dissolution. Graphene oxide (GO) was first obtained by a modified Hummer's method. Then through a hydrothermal treatment, GO was simultaneously reduced and assembled into a three-dimensional (3D) self-supported graphene framework (GF) after freeze-drying (Figure 2a). Such a macroscopic graphene foam was then directly used as support electrode to store metallic Li. Highly crumbled graphene nanoflakes constructed an interconnected network with hierarchical pores, which provided a large space to accommodate Li metal and electrolyte (Figure 2b). The pore volume was 1.6 mL g^{-1}, and the average pore size was 10 nm (Figure S1). The high-magnification scanning electron microscopy (SEM) images further indicated the thin-layer nature and 2D morphology of the graphene nanosheets (Figure S2a,b). It should be noticed that as-obtained chemically derived graphene possesses a high density of structural defects, which is beneficial for the nucleation of deposited Li.[41]

The entrapment of Li metal in nanoporous graphene was confirmed by SEM images of the SCG anode under completely lithiated and delithiated conditions. After being completely lithiated in the first cycle, graphene nanoflakes were conformally coated by metallic Li and the interspace pores were entirely filled up with Li metal (Figure 2c). More importantly, no sharp dendrite-like structure was observed except for some small perturbations with smooth tips that might be inherited from the graphene edges. After the subsequent delithiation, the nanoporous structure of the GF was recovered with 2D graphene nanosheets partially exposed (Figure 2d). The reversibility of deposited Li was thereby indicated. Compared to pristine GF, there was a smooth layer covering the surface of the graphene nanosheets, which was presumably assigned to *in situ* formed SEI and was identified in subsequent demonstration by XPS. Thus, we can conclude that

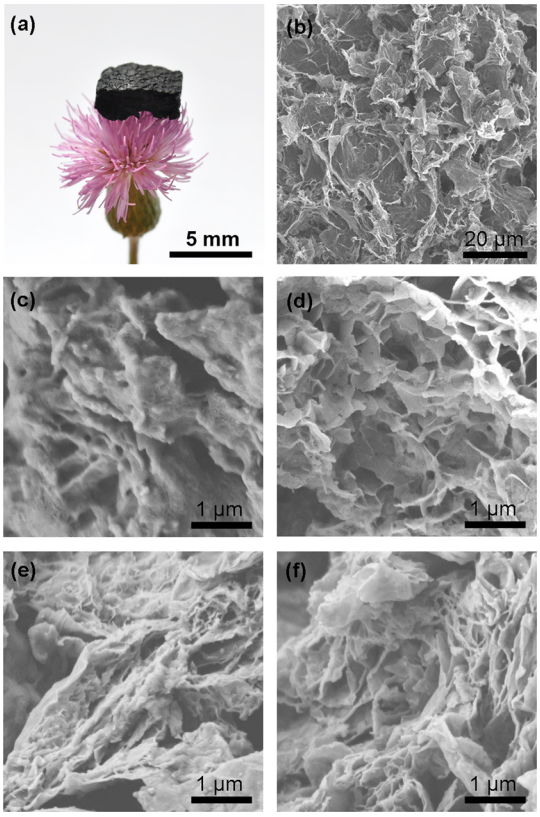

Figure 2. Morphology of the 3D GF during Li deposition and dissolution. (a) Side-view optical image of bulk GF on a flower. (b) SEM image of GF with large pores between the graphene sheets. (c−f) Morphology of SEM images of the SCG anode during the lithiation and delithiation process: (c) first and (e) 10th deposition; (d) first and (f) 10th dissolution.

metallic Li could reversibly deposit into/extract from nanopores of interspace graphene with the protection of an SEI layer on graphene nanosheets. These observations were further confirmed in the following 10 cycles (Figure 2e and f). Even after 10 lithiation/delithiation cycles, the interspace pores were still well preserved with no inert SEI layer blocking them (Figure 2f). Meanwhile, the self-supported, interconnected structure of GF was also maintained, indicating a good structural stability of the GF to sustain stress fluctuations.

TEM Characterization of Li Deposition in the SCG Framework. To further understand the Li deposition phenomenon in the SCG anode, high-resolution transmission electron microscopy (TEM) experiments were conducted. As Li metal has a low melting point, it is easy to melt into liquid under electron beam irradiation in TEM observations. When the electron dose was small (6240 e^- nm^{-2} s^{-1}), Li deposits were clearly observed in the SCG anode. A yolk−shell structure with an SCG coating on the Li deposits and graphene framework was determined (Figure 3a). After a high electron dose on the circular area (7.3×10^6 e^- nm^{-2}), the solid-state Li metal melted and disappeared gradually. The graphene nanosheets in the composite anode were

unambiguously identified (Figure 3b). However, a high-definition image and lattice image of graphene cannot be collected due to the encapsulating SEI layer and unfixed free-standing graphene flakes (Figure S2c). There was a sharp increase in the content of carbon element from 35% to 64% in the area of interest before and after the strong electron-beam exposure, indicating that graphene was preserved under strong electron-beam irradiation. When the electron dose was larger than 2.2×10^7 e^- nm^{-2} (corresponding to 1 h TEM observation in our case), the sample was completely different from the initial state. The solid-state Li was nearly all liquefied (Figure 3c). However, the SEI layers were well preserved, and more graphene frameworks were exposed. There was little structural damage on the SEI layers in the composite anode after Li dissolution (Figure S3). The stable SEI layer guaranteed stable Li deposition in the SCG anode. The thin SEI layer of 10 nm (Figure 3d) decreased the diffusion resistance of Li ions crossing through it, thus improving the rate performance of the Li metal anode. The stable and thin SEI layer was expected to afford a superior cycling performance of the SCG anode, which was investigated by the electrochemical performance evaluation.

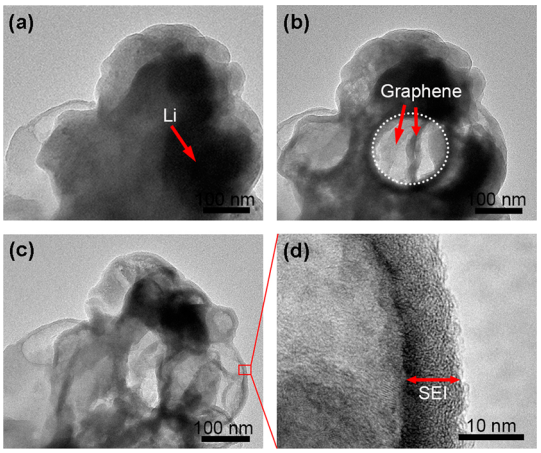

Figure 3. TEM images of the SCG anode with Li deposits. (a) Very low dose TEM image of Li depositing in the SCG anode. (b) After a high electron dose, liquid lithium disappeared and graphene was exposed under TEM. (c) The solid-state lithium was almostly liquefied after 1.0 h electron beam irradition. The SEI layer can be identified clearly. (d) High-resolution TEM image of the SEI layer in (c).

Resistance Characterization for the SCG Anode. The electrical impedance spectrum was employed to probe the electrodes of both pristine and lithiated SCG and the control electrode of Cu foil (Figure 4a). Both the bulk and interfacial impedances decreased sharply for the SCG-reinforced cells compared to the routine cells with Cu foil. An appropriate electric equivalent circuit was employed to interpret the Nyquist plots, in which R_Ω at the higher frequency represents the electrolyte resistance, while R_{CT} at the lower frequency represents the Li ion transfer resistance (Figure S4). The SCG electrode exhibited an R_Ω of 0.45 and 1.21 Ω before and after lithiation, while the two values were 0.95 and 3.25 Ω for the controlled metal electrodes on Cu foil (Figure 4b). Therefore, an improved ion transport behavior can be

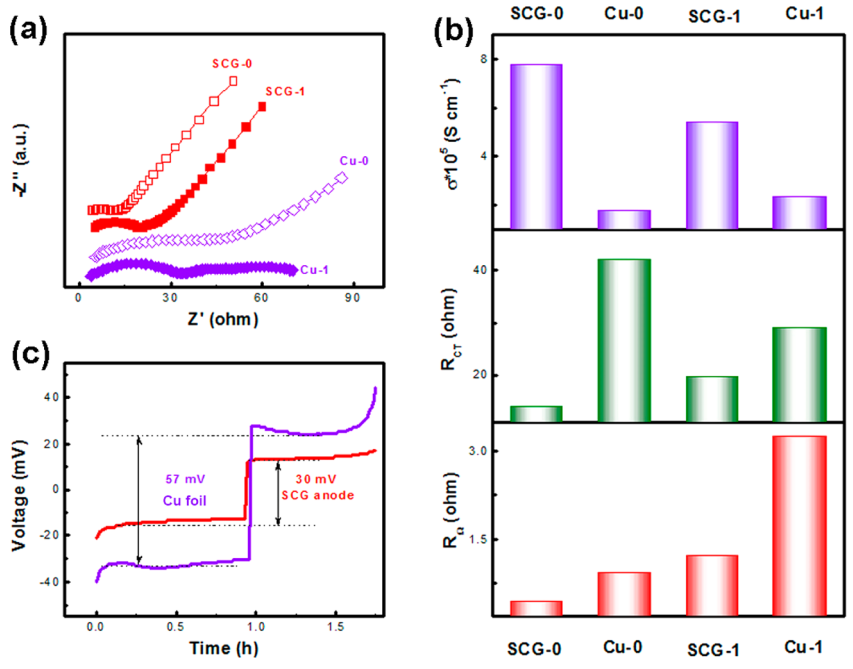

Figure 4. Li ion diffusion resistance through the Li metal anode. (a) Nyquist plots of pristine (marked as "0") and lithiated (marked as "1") SCG and Li anode on Cu foil. (b) R_Ω, R_C, and the electronical conductivities (σ) of pristine and lithiated graphene and a Cu foil based anode according to $\sigma = L/(RA)$, where L, A, and R are the thickness, area, and fitted resistance of electrode pellets. (c) Particle charge−discharge curves of SCG and a Cu foil based Li metal anode.

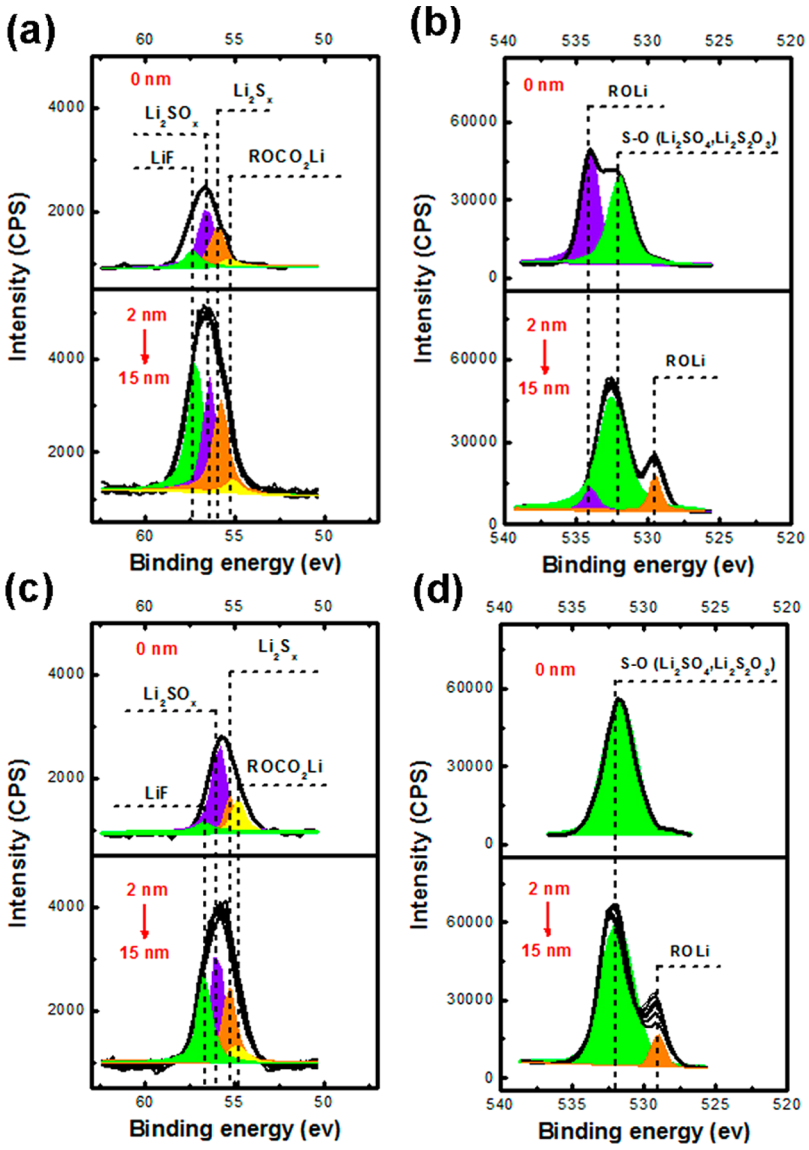

Figure 5. XPS characterization of the SCG anode. (a) Li 1s and (b) O 1s XPS spectra of the SEI layer from the lithium anode surface to a depth of 15 nm after the 10th lithiation. (c) Li 1s and (d) O 1s XPS spectra of the SEI layer from the lithium anode surface to a depth of 15 nm after the 10th delithiation.

suggested for SCG electrodes. The SCG electrode also delivered a small resistance of R_{CT} = 14.04 and 19.65 Ω before and after lithiation than those of the Li electrodes on Cu foils, with an R_{CT} of 42.12 and 29.10 Ω, respectively. According to the equation $\sigma = L/(RA)$, where L, A, and R are the thickness, area, and fitted resistance of electrode pellets, respectively,[65] the electrical conductivities (σ) of the electrodes were calculated as 7.81×10^{-2} and 5.42×10^{-2} mS cm^{-1} for the working SCG cell before and after lithiation, while for the cell with a Cu foil current collector, the values were much smaller, at 1.75×10^{-2} and 2.33×10^{-2} mS cm^{-1}. Such a decrease in electron/ion transfer resistance indicated that the SCG dual-phase structure can effectively prevent the formation of a mossy and inert interphase by retarding the accumulation of SEI compounds and recycling dead Li.

The improvement on interfacial transporting behavior by employing the SCG dual-phase structure was also confirmed by reduced polarization (hysteresis) in the voltage profile (Figure 4c). The voltage deviation of the SCG anode and Li electrode on Cu foil was 30 and 57 mV, respectively, which was in good accordance with the much reduced impedance for the SCG electrodes.

Component Analysis of SEI. To understand the chemical environment of the surface film on the cycled electrodes (Figure 2d and f), both the chemical composition and corresponding depth profile of the surface film were probed by XPS-equipped Ar ion sputtering. The chemical composition of the top layer (0 nm) was a little different from the bottom layer (2−15 nm) of the SEI film. For the Li 1s and O 1s spectra, the peaks were assigned to products of lithium bis(trifluoromethanesulfonyl)imide

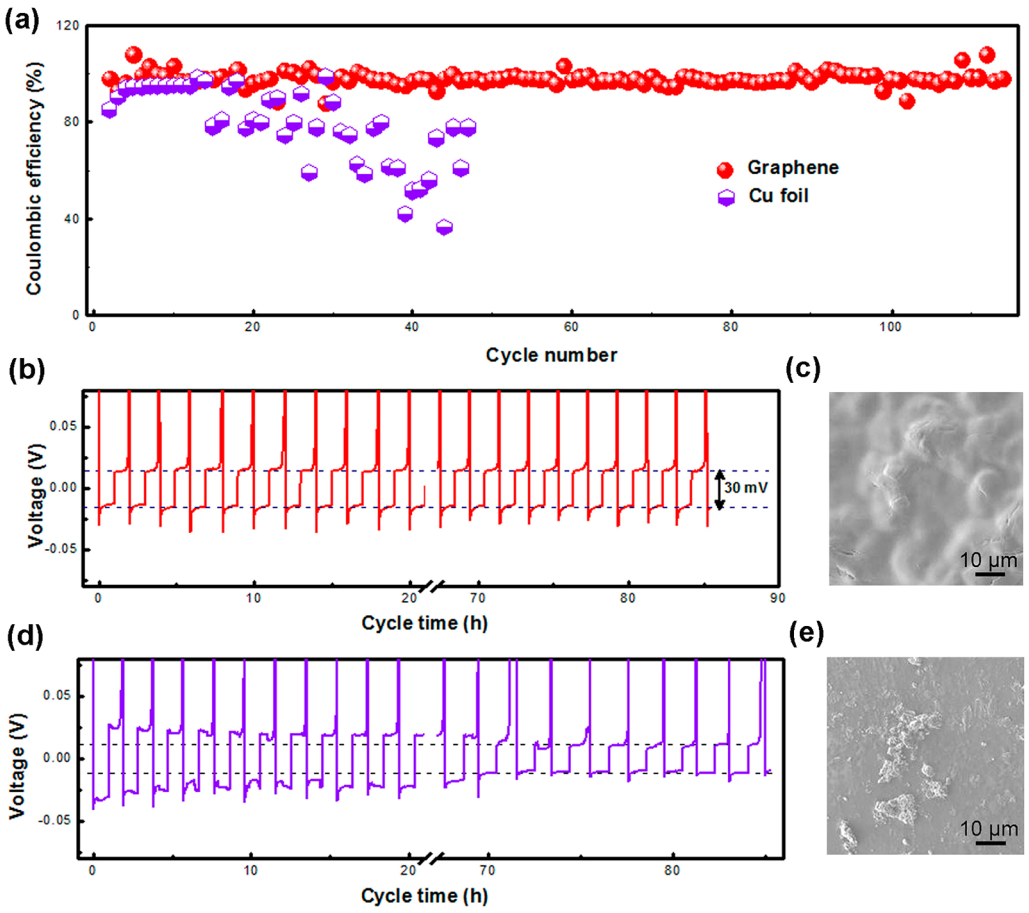

Figure 6. Electrochemical characterization of the electrodes for Li deposition/dissolution. (a) Coulombic efficiency of SCG and Cu foil based anode with a lithiation capacity of 0.5 mA h cm^{-2} at a current of 0.5 mA cm^{-2} (1.0 C). The voltage−time curves in an 86 h cycle of (b) SCG and (d) Cu foil based anode. The SEM images of the electrodes of (c) graphene and (e) Cu foil based anode after 86 h cycles.

(LiTFSI) and polysulfides decomposed on the Li electrode, such as $ROCO_2Li$ (54.6 eV), Li_2S_x (55.3 eV), Li_2SO_x (55.9 eV), and LiF (56.7 eV) in the Li 1s spectra, as well as ROLi (529, 533.6 eV) and S−O (Li_2SO_4, $Li_2S_2O_3$) (532 eV) in the O 1s spectra.[34,64,66,67] It can be speculated that the SEI after Li deposition here includes LiF, Li_2S_x, and Li_2SO_x (Figure 5a and b). The S 2p spectra in Figure S5 also confirmed these results. LiF might be the product of the reaction between LiTFSI and Li ions.[34] It plays a critical role in the formation of stable SEI with improved stability of Li electrodeposition.[18,55] The compounds of S−O (Li_2SO_4, $Li_2S_2O_3$) were obtained by the oxidation of LiTFSI and polysulfides by the oxidizing agent of $LiNO_3$ in the electrolyte. Li_2S_8 in the electrolyte was reduced into the lower order polysulfides, such as Li_2S_2 and Li_2S, which held a low solubility in the electrolyte and deposited on the anode as the SEI layer. To verify the stability of the SEI layer, both the chemical composition and the depth profile information on the surface film after Li dissolution were obtained. A similar result was obtained by the Li 1s, O 1s (Figure 5c and d), and S 2p spectra (Figure S5) after Li extraction. Therefore, the SEI layer retained a stable chemical composition and structure in both the lithiation/delithiation state.

The SEI is of prime importance to improve the Coulombic efficiency by separating the electrolyte and Li metal to inhibit the side reaction. When we removed the additives from the electrolyte, a decrease of 5% in the Coulombic efficiency was observed (Figure S6). There was a hysteresis in the voltage of about 38 mV for the SCG anode without electrolyte additives, which is 8 mV larger than the SCG anode with electrolyte additives. Thus, beyond the roles of the desolvation of Li ions and a physical barrier between the electrolyte and the Li metal anode, the polysulfide additives may also act as the catalyst to decrease the activation energy of Li ions crossing the SEI and depositing on the anode.[56,68]

Electrochemical Tests of LMBs. The electrochemical performance of the dual-phase SCG anode was demonstrated with Li metal foil as counter electrodes in coin cells. For LMBs, the Coulombic efficiency was a formidably important parameter to evaluate the sustainability of the specific anode. It was defined as the ratio of Li that was stripped out of the working electrode to the Li that was plated during each cycle. With a constant injection of charge, higher Coulombic efficiency indicated larger reversible capacity and reusable Li.

Li was electrochemically deposited from the Li metal counter electrode onto the SCG electrode and then stripped away in a half-cell. The current density was set as 1.0 C (0.5 mA cm^{-2} for a constant charge capacity of 0.5 mAh cm^{-2}). The Coulombic efficiency of the SCG electrode was maintained at ~97% for more than 100 cycles (Figure 6a), while the control sample with Cu foil exhibited a continuous degradation in Coulombic efficiency. The fading trend of Coulombic efficiency declined to lower than 40% after only 40 cycles. Note that the Coulombic efficiency of the Li electrode on Cu foil suffered from severe fluctuations, which was attributed to the reactivation of disconnected mossy Li from previous cycles. When a high current density of 1.0 and 2.0 mA cm^{-2} (2.0 and 4.0 C), which commonly induced low efficiency and rapid dendrite growth, was applied, the Coulombic efficiency of the Li/SCG anode was still maintained at ~93% (Figure S7). The temporal voltage profiles in Figure 6b exhibited stable lithiation/delithiation behaviors for the SCG anode as the nearly constant hysteresis indicated. The cycled Li/SCG anode delivered a smooth surface without visible dendrites (Figure 6c). In contrast, the voltage profiles of the controlled Li/Cu-based anode predominantly and irregularly fluctuated with many partial short-circuits during the long-term cycling (Figure 6d). There were large amounts of visible dendrites and dead Li on the surface after cycling (Figure 6e). The dendrite-inhibition behavior was more clearly demonstrated in a special cell configuration with a Teflon ring instead of the routine Cellgard 2400 membrane through overcharging cells at 0.5 mA cm^{-2} (Figure S8a).[55] The graphene-based anode demonstrated a superior dendrite-inhibition behavior in the 70 h lithiation process, while the cell with a Cu foil based anode was short-circuited after only 4 h of lithiation (Figure S8b,c). Li ions first deposited in the graphene framework within the anode and then on the graphene when the cell was overcharged (Figure S8d). The metal luster morphology of the overcharged anode indicated a dendrite-free deposition characterization. However, without a graphene framework, the short circuit early on led to little Li deposits on the metal anodes with Cu foils (Figure S8e). It was noted that a polysulfide stabilizer was also used for Li electrodes on Cu foils, which suggested that the structure evolution underneath the Li surface had a negative impact on the surface structure. The vital role of graphene on improving the subsurface transfer behavior of the Li metal anode was thereby illustrated.

To investigate the superlong cycling performance of the graphene anode, a 2000-cycle systematic test was conducted with 10 mAh cm^{-2} lithiation in the first cycle and 0.5 mAh cm^{-2} deposition/dissolution in the following cycles. Clearly, the SCG metal anode showed a stable cycling performance, while the Li anode on Cu foil had several instabilities in the voltage−time curve

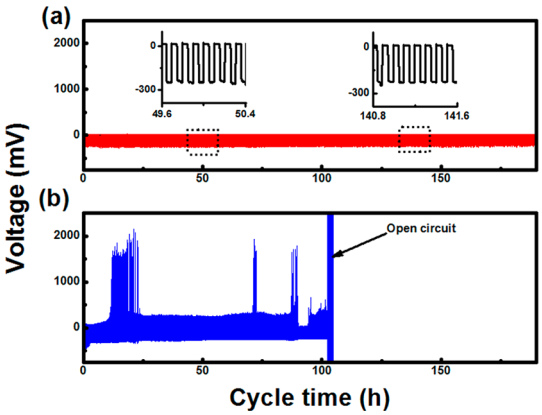

Figure 7. The 2000-cycle performance of (a) SCG and (b) Cu foil based Li metal anodes at a current density of 10 mA cm^{-2} with a prelithiation of 10.0 mAh cm^{-2}. The top curves in (a) are expanded views from the bottom plot.

(Figure 7). Especially, after 1000 cycles (100 h), the cell with a Cu based metal anode could no longer work because of the depletion of the electrolyte, indicating that the SEI on the Cu-based metal anode was always changing, leading to vast consumption of electrolyte. The advantages of the SCG anode can also be demonstrated when comparing the asymmetric cells of the SCG anode *vs* Li with symmetric cells of Li *vs* Li, because the Li plate exhibited a large decrease in voltage after 17 h, indicating the existence of a dendrite-induced short-circuit (Figure S9). The distinctive SCG metal anode with *in situ* formed SEI coated on the porous and interconnected graphene framework maintained the stability of the electrodes when Li ions transferred through the SEI layer and deposited in the anode efficiently and reversibly. The stable and thin SEI layer acted as the separator of the electrolyte and Li metal to inhibit the side reaction to improve the Coulombic efficiency and also as the accelerator of Li ions with superior conductivity for an excellent rate performance. The graphene framework not only inhibits the growth of "outward and dominant" Li dendrites but also handles the issues of poor lifespan caused by the "inward and recessive" diffusion resistance of Li ions before the dendrite-induced short-circuit. Consequently, the distinctive SCG structure reported herein provided a general strategy to settle the bottleneck issue of the anode of Li−S batteries.

CONCLUSIONS

We have illustrated a distinctive SCG structure for the anode of a Li−S battery with high safety and efficiency performance. The efficient *in situ* formed SEI-coated graphene structure allows a stable Li metal anode with a cycling Coulombic efficiency of ~97% for more than 100 cycles at 1.0 C and 93% at a higher current density of 2.0 and 4.0 C with dendrite-free morphology. The SCG structure indicates a low resistance and a high ion conductivity of 7.81×10^{-2} mS cm^{-1} with a nearly

5-fold increase relative to the Li anode on a Cu foil current collector. The stable and efficient Li deposition can be maintained for 2000 cycles. Future research is required to further improve the Coulombic efficiency and ion conductivity of Li metal anodes and investigate the diffusion of Li ions before and after crossing the SEI for the applications of Li–S batteries *via* the wise combination of nanoscale engineering and electrochemistry. We believe that the nanoengineering concepts described herein shed new light on high-energy-density LMBs, such as lithium–sulfur and lithium–oxygen batteries.

EXPERIMENTAL SECTION

Materials. The Li metal counter electrode is commercially available from China Energy Lithium Co., Ltd. The ether-based electrolyte composed of lithium bis(trifluoromethanesulfonyl)-imide (1.0 M) and 1,3-dioxolane/1,2-dimethoxyethane with a volumetric ratio of 1:1 was purchased from Zhangjiagang Guotai Huarong Chemical New Material Co., Ltd. To prepare the polysulfide additive, elemental S and pure Li_2S purchased from Alfa Aesar were mixed in a stoichiometric proportion to obtain Li_2S_8 (0.1 M), dissolving in the ester-based electrolytes.

Synthesis of a Graphene Framework. The porous GF was obtained by hydrothermal reduction of graphene oxide. The GO was prepared by a modified Hummers method.[69] The aqueous dispersion of 2.0 mg mL^{-1} GO was reduced by 90 mg mL^{-1} $NaHSO_3$ at 95 °C for 6.0 h without stirring to get a graphene hydrogel, which was further dialyzed against deionized water for 3 days to remove impurities.

Structure Characterizations. The morphology of the graphene was characterized by a JSM 7401F SEM operated at 3.0 kV and a JEM 2100 TEM operated at 120.0 kV. The N_2 adsorption–desorption isotherms were obtained using an N_2 adsorption analyzer (Autosorb-IQ_2-MP-C system) by N_2 adsorption at 77 K. The specific surface area of all samples was calculated by the BET method. The pore size distribution plots were obtained by the nonlinear density functional theory method. Al-Kα radiation (72 W, 12 kV) at a pressure of 10^{-9} Torr was used to obtain the X-ray photoelectron spectra. The diameter of the analyzed area was 400 mm. An argon ion beam (accelerating voltage 2.0 keV, ion beam current 6.0 mA) was employed to perform the etching process. The etching rate was estimated as 0.007 nm s^{-1}, and after 2130 s, nearly a 15 nm surface layer was etched. The metal anode sample were prepard in a glovebox and protected under Ar to avoid oxidation and other secondary reactions.

Electrochemical Measurement. A two-electrode cell configuration using standard 2025 coin-type cells was employed. The two-electrode cells were assembled in an Ar-filled glovebox with O_2 and H_2O content below 1 ppm. A homogeneously slurry was prepared by mixing GF and polyvinylidene difluoride (PVDF) binder in *N*-methylpyrrolidinone with a mass ratio of GF:PVDF = 90:10, followed by magnetic stirring for *ca.* 24.0 h. The slurry was coated onto a Cu foil and dried in a vacuum drying oven at 60 °C for 6.0 h. The as-obtained foil was punched into 13.0 mm disks as the working electrodes. A 1.0 mm thick Li metal foil was employed as the counter electrode, and Li_2S_8 (0.1 M) and $LiNO_3$ (1.0%) dissolved in the ether-based electrolytes served as the electrolyte. The coin cells were monitored in galvanostatic mode within a voltage range of −0.5 to 1.5 V using a Neware multichannel battery cycler. The EIS measurement was performed on a Solartron 1470E electrochemical workstation. It should be noted that the lithiation capacity was 0.5 mAh cm^{-2} at 0.5 mA cm^{-2} and the mass loading of graphene was 0.16 mg; thus the specific capacity of the electrode was 3086 mAh g^{-1} at 0.5 mA cm^{-2}, which was a large increase relative to the graphene anode in the Li ion batteries.

Conflict of Interest: The authors declare no competing financial interest.

Supporting Information Available: The N_2 isotherm, SEM and TEM images of the GF, schematic of the EIS, XPS characterization of the SCG anode, electrochemical characterization of the electrodes for Li deposition/dissolution, electrochemical characterization of high rate performance of the SCG anode, and dendrite-inhibition behavior of the graphene framework. The Supporting Information is available free of charge on the ACS Publications website at DOI: 10.1021/acsnano.5b01990.

Acknowledgment. This work was supported by the National Natural Science Foundation of China (21306103 and 21422604) and Tsinghua University Initiative Scientific Research Program (2014z22076).

REFERENCES AND NOTES

1. Goodenough, J. B. Electrochemical Energy Storage in a Sustainable Modern Society. *Energy Environ. Sci.* **2014**, *7*, 14–18.
2. Song, M. K.; Cairns, E. J.; Zhang, Y. G. Lithium/Sulfur Batteries with High Specific Energy: Old Challenges and New Opportunities. *Nanoscale* **2013**, *5*, 2186–2204.
3. Manthiram, A.; Chung, S.-H.; Zu, C. Lithium–Sulfur Batteries: Progress and Prospects. *Adv. Mater.* **2015**, *27*, 1980–2006.
4. Li, Z.; Huang, Y.; Yuan, L.; Hao, Z.; Huang, Y. Status and Prospects in Sulfur–Carbon Composites as Cathode Materials for Rechargeable Lithium–Sulfur Batteries. *Carbon* **2015**, *92*, 41–63.
5. Cheng, X.-B.; Huang, J.-Q.; Peng, H.-J.; Nie, J.-Q.; Liu, X.-Y.; Zhang, Q.; Wei, F. Polysulfide Shuttle Control: Towards a Lithium-Sulfur Battery with Superior Capacity Performance up to 1000 Cycles by Matching the Sulfur/Electrolyte Loading. *J. Power Sources* **2014**, *253*, 263–268.
6. Peng, H.-J.; Liang, J.; Zhu, L.; Huang, J.-Q.; Cheng, X.-B.; Guo, X.; Ding, W.; Zhu, W.; Zhang, Q. Catalytic Self-Limited Assembly at Hard Templates: A Mesoscale Approach to Graphene Nanoshells for Lithium–Sulfur Batteries. *ACS Nano* **2014**, *8*, 11280–11289.
7. Qu, Y.; Zhang, Z.; Wang, X.; Lai, Y.; Liu, Y.; Li, J. A Simple SDS-Assisted Self-Assembly Method for the Synthesis of Hollow Carbon Nanospheres to Encapsulate Sulfur for Advanced Lithium-Sulfur Batteries. *J. Mater. Chem. A* **2013**, *1*, 14306–14310.
8. Xu, J.; Shui, J.; Wang, J.; Wang, M.; Liu, H.-K.; Dou, S. X.; Jeon, I.-Y.; Seo, J.-M.; Baek, J.-B.; Dai, L. Sulfur–Graphene Nanostructured Cathodes *via* Ball-Milling for High-Performance Lithium–Sulfur Batteries. *ACS Nano* **2014**, *8*, 10920–10930.
9. Chen, H.; Wang, C.; Dong, W.; Lu, W.; Du, Z.; Chen, L. Monodispersed Sulfur Nanoparticles for Lithium–Sulfur Batteries with Theoretical Performance. *Nano Lett.* **2015**, *15*, 798–802.
10. Seh, Z. W.; Li, W.; Cha, J. J.; Zheng, G.; Yang, Y.; McDowell, M. T.; Hsu, P.-C.; Cui, Y. Sulphur–TiO_2 Yolk–Shell Nanoarchitecture with Internal Void Space for Long-Cycle Lithium–Sulphur Batteries. *Nat. Commun.* **2013**, *4*, 1331.
11. Song, J.; Gordin, M. L.; Xu, T.; Chen, S.; Yu, Z.; Sohn, H.; Lu, J.; Ren, Y.; Duan, Y.; Wang, D. Strong Lithium Polysulfide Chemisorption on Electroactive Sites of Nitrogen-Doped Carbon Composites for High-Performance Lithium–Sulfur Battery Cathodes. *Angew. Chem., Int. Ed.* **2015**, *54*, 4325–4329.
12. Zhao, M.-Q.; Sedran, M.; Ling, Z.; Lukatskaya, M. R.; Mashtalir, O.; Ghidiu, M.; Dyatkin, B.; Tallman, D. J.; Djenizian, T.; Barsoum, M. W.; *et al.* Synthesis of Carbon/Sulfur Nanolaminates by Electrochemical Extraction of Titanium from Ti_2SC. *Angew. Chem., Int. Ed.* **2015**, *54*, 4810–4814.
13. Song, J. X.; Xu, T.; Gordin, M. L.; Zhu, P. Y.; Lv, D. P.; Jiang, Y. B.; Chen, Y. S.; Duan, Y. H.; Wang, D. H. Nitrogen-Doped

Mesoporous Carbon Promoted Chemical Adsorption of Sulfur and Fabrication of High-Areal-Capacity Sulfur Cathode with Exceptional Cycling Stability for Lithium-Sulfur Batteries. *Adv. Funct. Mater.* **2014**, *24*, 1243–1250.
14. Tang, C.; Zhang, Q.; Zhao, M. Q.; Huang, J. Q.; Cheng, X. B.; Tian, G. L.; Peng, H. J.; Wei, F. Nitrogen-Doped Aligned Carbon Nanotube/Graphene Sandwiches: Facile Catalytic Growth on Bifunctional Natural Catalysts and Their Applications as Scaffolds for High-Rate Lithium-Sulfur Batteries. *Adv. Mater.* **2014**, *26*, 6100–6105.
15. Xiao, L.; Cao, Y.; Xiao, J.; Schwenzer, B.; Engelhard, M. H.; Saraf, L. V.; Nie, Z.; Exarhos, G. J.; Liu, J. A Soft Approach to Encapsulate Sulfur: Polyaniline Nanotubes for Lithium-Sulfur Batteries with Long Cycle Life. *Adv. Mater.* **2012**, *24*, 1176–1181.
16. Li, W.; Zhang, Q.; Zheng, G.; Seh, Z. W.; Yao, H.; Cui, Y. Understanding the Role of Different Conductive Polymers in Improving the Nanostructured Sulfur Cathode Performance. *Nano Lett.* **2013**, *13*, 5534–5540.
17. Wang, J.; Yang, J.; Xie, J.; Xu, N. A Novel Conductive Polymer–Sulfur Composite Cathode Material for Rechargeable Lithium Batteries. *Adv. Mater.* **2002**, *14*, 963–965.
18. Zhou, G.; Li, L.; Wang, D.-W.; Shan, X.-Y.; Pei, S.; Li, F.; Cheng, H.-M. A Flexible Sulfur-Graphene-Polypropylene Separator Integrated Electrode for Advanced Li–S Batteries. *Adv. Mater.* **2015**, *27*, 641–647.
19. Huang, J.-Q.; Zhang, Q.; Peng, H.-J.; Liu, X.-Y.; Qian, W.-Z.; Wei, F. Ionic Shield for Polysulfides Towards Highly-Stable Lithium-Sulfur Batteries. *Energy Environ. Sci.* **2014**, *7*, 347–353.
20. Su, Y.-S.; Manthiram, A. Lithium–Sulphur Batteries with a Microporous Carbon Paper as a Bifunctional Interlayer. *Nat. Commun.* **2012**, *3*, 1166.
21. Huang, J.-Q.; Zhuang, T.-Z.; Zhang, Q.; Peng, H.-J.; Chen, C.-M.; Wei, F. Permselective Graphene Oxide Membrane for Highly Stable and Anti-Self-Discharge Lithium–Sulfur Batteries. *ACS Nano* **2015**, *9*, 3002–3011.
22. Chung, S. H.; Manthiram, A. Bifunctional Separator with a Light-Weight Carbon-Coating for Dynamically and Statically Stable Lithium-Sulfur Batteries. *Adv. Funct. Mater.* **2014**, *24*, 5299–5306.
23. Xu, G.; Ding, B.; Pan, J.; Nie, P.; Shen, L.; Zhang, X. High Performance Lithium-Sulfur Batteries: Advances and Challenges. *J. Mater. Chem. A* **2014**, *2*, 12662–12676.
24. Barghamadi, M.; Best, A. S.; Bhatt, A. I.; Hollenkamp, A. F.; Musameh, M.; Rees, R. J.; Ruther, T. Lithium-Sulfur Batteries-The Solution Is in the Electrolyte, but Is the Electrolyte a Solution? *Energy Environ. Sci.* **2014**, *7*, 3902–3920.
25. Lin, Z.; Liang, C. Lithium-Sulfur Batteries: From Liquid to Solid Cells. *J. Mater. Chem. A* **2015**, *3*, 936–958.
26. Bresser, D.; Passerini, S.; Scrosati, B. Recent Progress and Remaining Challenges in Sulfur-Based Lithium Secondary Batteries - A Review. *Chem. Commun.* **2013**, *49*, 10545–10562.
27. Zhou, G. M.; Yin, L. C.; Wang, D. W.; Li, L.; Pei, S. F.; Gentle, I. R.; Li, F.; Cheng, H. M. Fibrous Hybrid of Graphene and Sulfur Nanocrystals for High-Performance Lithium-Sulfur Batteries. *ACS Nano* **2013**, *7*, 5367–5375.
28. Evers, S.; Nazar, L. F. New Approaches for High Energy Density Lithium–Sulfur Battery Cathodes. *Acc. Chem. Res.* **2013**, *46*, 1135–1143.
29. Yin, Y.-X.; Xin, S.; Guo, Y.-G.; Wan, L.-J. Lithium–Sulfur Batteries: Electrochemistry, Materials, and Prospects. *Angew. Chem., Int. Ed.* **2013**, *52*, 13186–13200.
30. Zhang, S. S. Liquid Electrolyte Lithium/Sulfur Battery: Fundamental Chemistry, Problems, and Solutions. *J. Power Sources* **2013**, *231*, 153–162.
31. Brückner, J.; Thieme, S.; Böttger-Hiller, F.; Bauer, I.; Grossmann, H. T.; Strubel, P.; Althues, H.; Spange, S.; Kaskel, S. Carbon-Based Anodes for Lithium Sulfur Full Cells with High Cycle Stability. *Adv. Funct. Mater.* **2014**, *24*, 1284–1289.
32. Xiong, S.; Xie, K.; Diao, Y.; Hong, X. On the Role of Polysulfides for a Stable Solid Electrolyte Interphase on the Lithium Anode Cycled in Lithium–Sulfur Batteries. *J. Power Sources* **2013**, *236*, 181–187.
33. Zu, C.; Manthiram, A. Stabilized Lithium–Metal Surface in a Polysulfide-Rich Environment of Lithium–Sulfur Batteries. *J. Phys. Chem. Lett.* **2014**, *5*, 2522–2527.
34. Aurbach, D.; Pollak, E.; Elazari, R.; Salitra, G.; Kelley, C. S.; Affinito, J. On the Surface Chemical Aspects of Very High Energy Density, Rechargeable Li-Sulfur Batteries. *J. Electrochem. Soc.* **2009**, *156*, A694–A702.
35. Suo, L.; Hu, Y.-S.; Li, H.; Armand, M.; Chen, L. A New Class of Solvent-in-Salt Electrolyte for High-Energy Rechargeable Metallic Lithium Batteries. *Nat. Commun.* **2013**, *4*, 1481.
36. Huang, C.; Xiao, J.; Shao, Y.; Zheng, J.; Bennett, W. D.; Lu, D.; Saraf, L. V.; Engelhard, M.; Ji, L.; Zhang, J.; Li, X.; Graff, G. L.; Liu, J. Manipulating Surface Reactions in Lithium-Sulphur Batteries Using Hybrid Anode Structures. *Nat. Commun.* **2014**, *5*, 3015.
37. Cheng, X.-B.; Peng, H.-J.; Huang, J.-Q.; Wei, F.; Zhang, Q. Dendrite-Free Nanostructured Anode: Entrapment of Lithium in a 3D Fibrous Matrix for Ultra-Stable Lithium–Sulfur Batteries. *Small* **2014**, *10*, 4257–4263.
38. Zhang, X.; Wang, W.; Wang, A.; Huang, Y.; Yuan, K.; Yu, Z.; Qiu, J.; Yang, Y. Improved Cycle Stability and High Security of Li-B Alloy Anode for Lithium-Sulfur Battery. *J. Mater. Chem. A* **2014**, *2*, 11660–11665.
39. Ma, G.; Wen, Z.; Wang, Q.; Shen, C.; Jin, J.; Wu, X. Enhanced Cycle Performance of a Li-S Battery Based on a Protected Lithium Anode. *J. Mater. Chem. A* **2014**, *2*, 19355–19359.
40. Wang, J. L.; Lin, F. J.; Jia, H.; Yang, J.; Monroe, C. W.; NuLi, Y. N. Towards a Safe Lithium-Sulfur Battery with a Flame-Inhibiting Electrolyte and a Sulfur-Based Composite Cathode. *Angew. Chem., Int. Ed.* **2014**, *53*, 10099–10104.
41. Mukherjee, R.; Thomas, A. V.; Datta, D.; Singh, E.; Li, J.; Eksik, O.; Shenoy, V. B.; Koratkar, N. Defect-Induced Plating of Lithium Metal within Porous Graphene Networks. *Nat. Commun.* **2014**, *5*, 3710.
42. Cao, R.; Xu, W.; Lv, D.; Xiao, J.; Zhang, J.-G. Anodes for Rechargeable Lithium-Sulfur Batteries. *Adv. Energy Mater.* **2015**, *5*, 1402273.
43. Whittingham, M. S. History, Evolution, and Future Status of Energy Storage. *Proc. IEEE* **2012**, *100*, 1518–1534.
44. Manthiram, A.; Fu, Y.; Chung, S.-H.; Zu, C.; Su, Y.-S. Rechargeable Lithium-Sulfur Batteries. *Chem. Rev.* **2014**, *114*, 11751–11787.
45. Cheng, X.-B.; Zhang, Q. Dendrite-Free Lithium Metal Anodes: Stable Solid Electrolyte Interphases for High-Efficiency Batteries. *J. Mater. Chem. A* **2015**, *3*, 7207–7209.
46. Whittingham, M. S. Lithium Batteries and Cathode Materials. *Chem. Rev.* **2004**, *104*, 4271–4302.
47. Richardson, T. J.; Chen, G. Solid Solution Lithium Alloy Cermet Anodes. *J. Power Sources* **2007**, *174*, 810–812.
48. Xu, K. Electrolytes and Interphases in Li-Ion Batteries and Beyond. *Chem. Rev.* **2014**, *114*, 11503–11618.
49. Brissot, C.; Rosso, M.; Chazalviel, J. N.; Baudry, P.; Lascaud, S. *In Situ* Study of Dendritic Growth in Lithium/Peo-Salt/Lithium Cells. *Electrochim. Acta* **1998**, *43*, 1569–1574.
50. Monroe, C.; Newman, J. The Impact of Elastic Deformation on Deposition Kinetics at Lithium/Polymer Interfaces. *J. Electrochem. Soc.* **2005**, *152*, A396–A404.
51. Rangasamy, E.; Liu, Z.; Gobet, M.; Pilar, K.; Sahu, G.; Zhou, W.; Wu, H.; Greenbaum, S.; Liang, C. An Iodide Based $Li_7P_2S_8I$ Superionic Conductor. *J. Am. Chem. Soc.* **2015**, *137*, 1384–1387.
52. Tu, Z. Y.; Kambe, Y.; Lu, Y. Y.; Archer, L. A. Nanoporous Polymer-Ceramic Composite Electrolytes for Lithium Metal Batteries. *Adv. Energy Mater.* **2014**, *4*, 1300654.
53. Yan, K.; Lee, H.-W.; Gao, T.; Zheng, G.; Yao, H.; Wang, H.; Lu, Z.; Zhou, Y.; Liang, Z.; Liu, Z. F.; *et al*. Ultrathin Two-Dimensional Atomic Crystals as Stable Interfacial Layer for Improvement of Lithium Metal Anode. *Nano Lett.* **2014**, *14*, 6016–6022.
54. Zheng, G.; Lee, S. W.; Liang, Z.; Lee, H.-W.; Yan, K.; Yao, H.; Wang, H.; Li, W.; Chu, S.; Cui, Y. Interconnected Hollow Carbon Nanospheres for Stable Lithium Metal Anodes. *Nat. Nanotechnol.* **2014**, *9*, 618–623.

55. Lu, Y.; Tu, Z.; Archer, L. A. Stable Lithium Electrodeposition in Liquid and Nanoporous Solid Electrolytes. *Nat. Mater.* **2014**, *13*, 961–969.
56. Miao, R.; Yang, J.; Feng, X.; Jia, H.; Wang, J.; Nuli, Y. Novel Dual-Salts Electrolyte Solution for Dendrite-Free Lithium-Metal Based Rechargeable Batteries with High Cycle Reversibility. *J. Power Sources* **2014**, *271*, 291–297.
57. Qian, J.; Henderson, W. A.; Xu, W.; Bhattacharya, P.; Engelhard, M.; Borodin, O.; Zhang, J.-G. High Rate and Stable Cycling of Lithium Metal Anode. *Nat. Commun.* **2015**, *6*, 6362.
58. Ding, F.; Xu, W.; Graff, G. L.; Zhang, J.; Sushko, M. L.; Chen, X.; Shao, Y.; Engelhard, M. H.; Nie, Z.; Xiao, J.; *et al*. Dendrite-Free Lithium Deposition *via* Self-Healing Electrostatic Shield Mechanism. *J. Am. Chem. Soc.* **2013**, *135*, 4450–4456.
59. Khurana, R.; Schaefer, J. L.; Archer, L. A.; Coates, G. W. Suppression of Lithium Dendrite Growth Using Cross-Linked Polyethylene/Poly(ethylene oxide) Electrolytes: A New Approach for Practical Lithium-Metal Polymer Batteries. *J. Am. Chem. Soc.* **2014**, *136*, 7395–7402.
60. Ryou, M.-H.; Lee, Y. M.; Lee, Y.; Winter, M.; Bieker, P. Mechanical Surface Modification of Lithium Metal: Towards Improved Li Metal Anode Performance by Directed Li Plating. *Adv. Funct. Mater.* **2015**, *25*, 834–841.
61. Liang, Z.; Zheng, G. Y.; Liu, C.; Liu, N.; Li, W. Y.; Yan, K.; Yao, H. B.; Hsu, P. C.; Chu, S.; Cui, Y. Polymer Nanofiber-Guided Uniform Lithium Deposition for Battery Electrodes. *Nano Lett.* **2015**, *15*, 2910–2916.
62. Harry, K. J.; Hallinan, D. T.; Parkinson, D. Y.; MacDowell, A. A.; Balsara, N. P. Detection of Subsurface Structures Underneath Dendrites Formed on Cycled Lithium Metal Electrodes. *Nat. Mater.* **2014**, *13*, 69–73.
63. Lv, D.; Shao, Y.; Lozano, T.; Bennett, W. D.; Graff, G. L.; Polzin, B.; Zhang, J.; Engelhard, M. H.; Saenz, N. T.; Henderson, W. A.; *et al*. Failure Mechanism for Fast-Charged Lithium Metal Batteries with Liquid Electrolytes. *Adv. Energy Mater.* **2015**, *5*, 1400993.
64. Xiong, S.; Xie, K.; Diao, Y.; Hong, X. Characterization of the Solid Electrolyte Interphase on Lithium Anode for Preventing the Shuttle Mechanism in Lithium−Sulfur Batteries. *J. Power Sources* **2014**, *246*, 840–845.
65. Wang, B.; Wu, X.-L.; Shu, C.-Y.; Guo, Y.-G.; Wang, C.-R. Synthesis of CuO/Graphene Nanocomposite as a High-Performance Anode Material for Lithium-Ion Batteries. *J. Mater. Chem.* **2010**, *20*, 10661–10664.
66. Diao, Y.; Xie, K.; Xiong, S. Z.; Hong, X. B. Insights into Li-S Battery Cathode Capacity Fading Mechanisms: Irreversible Oxidation of Active Mass during Cycling. *J. Electrochem. Soc.* **2012**, *159*, A1816–A1821.
67. Wu, Z.-S.; Xue, L.; Ren, W.; Li, F.; Wen, L.; Cheng, H.-M. A LiF Nanoparticle-Modified Graphene Electrode for High-Power and High-Energy Lithium Ion Batteries. *Adv. Funct. Mater.* **2012**, *22*, 3290–3297.
68. Shkrob, I. A.; Marin, T. W.; Zhu, Y.; Abraham, D. P. Why Bis(fluorosulfonyl)imide Is a "Magic Anion" for Electrochemistry. *J. Phys. Chem. C* **2014**, *118*, 19661–19671.
69. Wang, Y.-X.; Huang, L.; Sun, L.-C.; Xie, S.-Y.; Xu, G.-L.; Chen, S.-R.; Xu, Y.-F.; Li, J.-T.; Chou, S.-L.; Dou, S.-X.; *et al*. Facile Synthesis of a Interleaved Expanded Graphite-Embedded Sulphur Nanocomposite as Cathode of Li-S Batteries with Excellent Lithium Storage Performance. *J. Mater. Chem.* **2012**, *22*, 4744–4750.